Quatorzième édition des Journées scientifiques
du Regroupement francophone pour la recherche et la formation sur le béton
$(RF)^2B$

Sherbrooke, Québec, Canada
22-23 août 2013

APPROCHE MACRO-CINEMATIQUE POUR LA MODELISATION DE POUTRES-VOILE CONTINUES

B. Mihaylov
Département ArGEnCo : Secteur Structural Engineering, Université de Liège, Liège, Belgique

RÉSUMÉ : Cet article présente une approche macro-cinématique permettant de décrire les schémas de déformation avec fissures diagonales des poutres-voile continues. On montre comment une poutre continue formée de deux travées symétriques et supportant deux charges concentrées égales peut être modélisée à partir de seulement deux degrés de liberté. Ce modèle cinématique est combiné avec une théorie cinématique à trois paramètres (3PKT) qui permet de calculer la résistance au cisaillement de poutres-voile, les réactions d'appuis à la ruine et la capacité de déformation de poutres-voile continues. Cette approche a été appliquée à quatorze essais de cisaillement issus de la littérature avec différentes hauteurs de section, différents arrangement de l'armaturage longitudinal et différentes quantités d'armaturage de cisaillement. Les résultats montrent que cette approche macro-cinématique basée sur deux degrés de liberté reproduit correctement les tendances observées dans la capacité ultime au cisaillement des spécimens.

1. INTRODUCTION

Continuous reinforced concrete beams with small span-to-depth ratios (deep beams) find important applications in the structures of buildings and bridges. Examples of such members are deep transfer girders above large open spaces in high-rise buildings and deep cap beams in bridge pier bents. Deep beams are characterised by complex deformation patterns and cannot be modelled based on the classical plane-sections-remain-plane assumption. The strength of deep beams is typically evaluated by using strut-and-tie models (CSA Committee A23.3 2004, ACI Committee 318 2011, CEN 2004) which usually provide conservative predictions. However, as strut-and-tie models consider mainly equilibrium, they are not well suited for evaluating deformations. Calculation of deformations can be performed by using non-linear finite element models (FEM) which account for concrete cracking as well as plastic deformations in the concrete and the steel (Vecchio 2001). In order to capture the deformation patterns in deep beams, however, FE models must use thousands of degrees of freedom (DOFs) and require significant time for modelling and analysis.

This paper will discuss an alternative approach which is based on a simple but accurate kinematic description of the deformation patterns in continuous deep beams (Mihaylov et al., 2013a and 2013b). It will be shown that with this macro-kinematic approach a symmetrical two-span deep beam supporting two equal point loads can be modelled with the help of only two degrees of freedom. The capabilities of the model will be demonstrated through comparisons with fourteen tests of continuous deep beams from the literature.

2. MODELLING THE DEFORMATION PATTERNS IN DEEP BEAMS

Figure 1 shows a three-parameter kinematic model for the deformation patterns in diagonally-cracked shear spans of deep beams under point loads (Mihaylov et al. 2013a and 2013b). The shear span is bound between a point load applied on the top face of the member and a support reaction on the bottom face. The model assumes that deep shear spans develop two major shear cracks and that one of these cracks opens at shear failure. The bottom shear crack extends from the inner edge of the support to the point along the width of the loading element where the shear force is zero. Inversely, the top crack runs between the inner edge of the loading element and the point along the width of the support where the shear is zero. The cracked concrete above and below the two major cracks is modelled by two "fans" of rigid struts between radial cracks. The struts of the bottom fan are connected to the bottom reinforcement and are pinned at the loading point while those of the top fan are connected to the top reinforcement and join at the support. In more slender beams the angle of the flattest strut, and similarly the angle of the major shear cracks α_1, is limited to the angle θ of the shear cracks that develop in a uniform stress field undisturbed by point loads and support reactions:

(1) $\sim_1 = \sim \geq^{-}$

Where α is the angle of the line connecting the loading and support points. In slender beams under double curvature an undisturbed field forms between the two fans. Angle θ can be calculated from the shear provisions of the Canadian code (CSA Committee A23.3 2004) or it can be taken equal to 30˚.

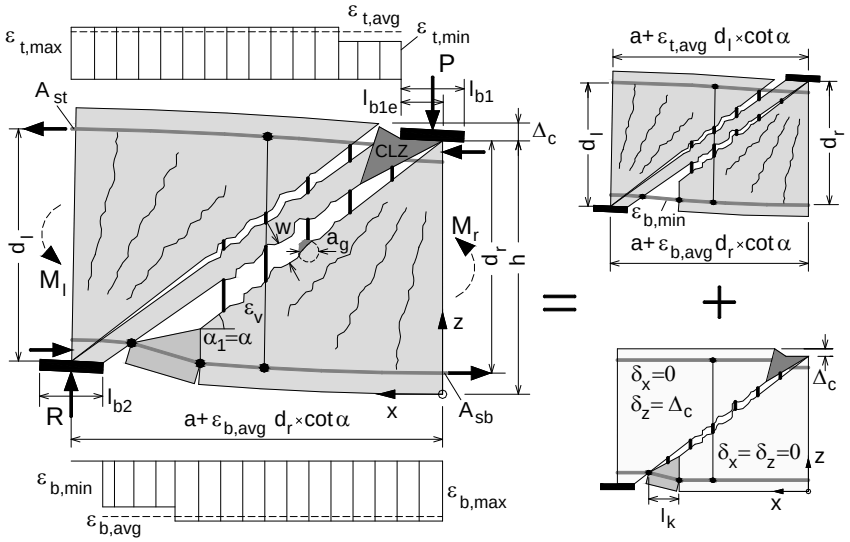

Figure 1. Three-parameter kinematic model for deep beams (Mihaylov et al. 2013a and 2013b).

As shown in Figure 1, the complete deformation pattern of the shear span is obtained as a superposition of two deformation patterns. The top pattern is associated with the elongation of the top and bottom longitudinal reinforcements (average strains $\varepsilon_{t,avg}$ and $\varepsilon_{b,avg}$, respectively) while the bottom pattern depends on the transverse displacement Δ_c of the critical loading zone (CLZ). Namely deformations $\varepsilon_{b,avg}$, $\varepsilon_{t,avg}$, and Δ_c are the three independent kinematic parameters (degrees of freedom) of the kinematic model. In the top deformation pattern the radial struts rotate with respect to each other and the cracks between them widen as the longitudinal reinforcement stretches. In the bottom pattern, on the other hand, the critical diagonal crack widens and slips as the CLZ deforms transversally to the axis of the member. If the values of $\varepsilon_{b,avg}$, $\varepsilon_{t,avg}$, and Δ_c are known, the complete displacement field of a deep shear span can be obtained based on the assumptions of the kinematic model:

- Points below the critical diagonal crack

(2) $¢_x = £_{b,avg} x$

(3) $¢_z = \dfrac{£_{b,avg} x^2}{h - z}$

- Points above the critical diagonal crack

(4) $¢_x = £_{b,avg}(h - z)\cot\sim + £_{t,avg}(x - a + z\cot\sim)$*

(5) $¢_z = £_{b,avg} x\cot\sim + \Delta_c + £_{t,avg}(x - a + z\cot\sim)(a - x)/z$ *

Where the terms marked with asterisks apply only to points with z coordinates larger than (a-x) tan α_1. These equations represent conditions for compatibility of the deformations in the shear span. They can be used to derive important deformations such as the strain in the transverse reinforcement ε_v and, with some additional assumptions related to the contribution of strain $\varepsilon_{b,min}$, the width of the critical diagonal crack *w* (Mihaylov et al., 2013a). These deformations are again a function of the three unknown degrees of freedom of the kinematic model.

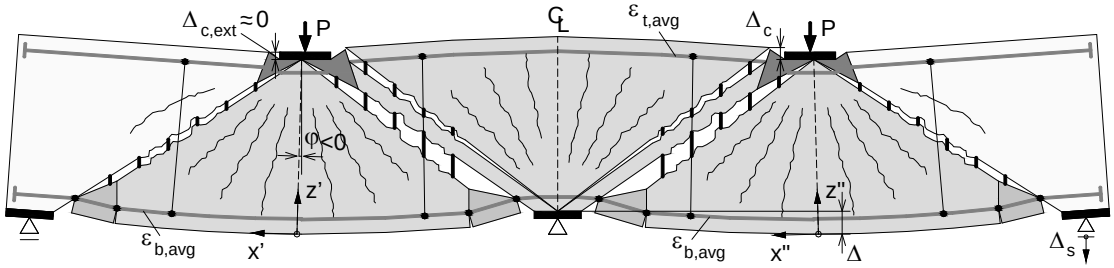

a) Kinematic model

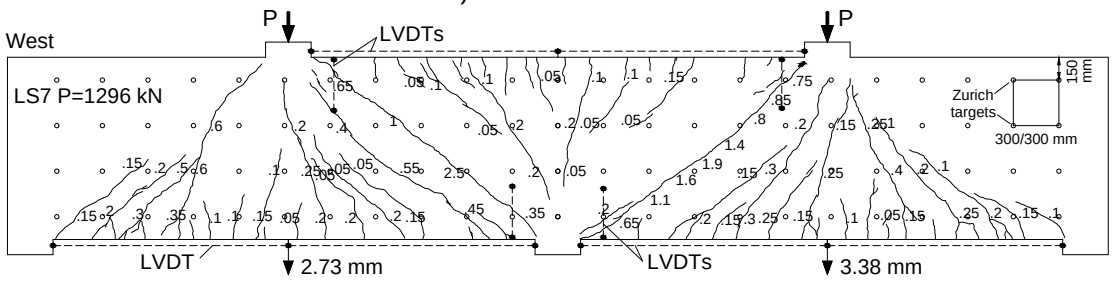

b) Crack diagram at shear failure (crack widths in mm) - test CDB1 (Mihaylov et al., 2013b)

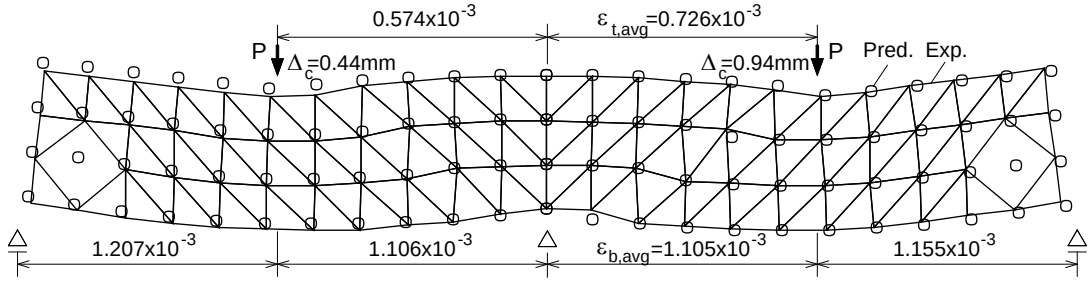

c) Measured and predicted deformed shapes at shear failure

Figure 2. Kinematic modelling of a symmetrical deep beam.

Figure 2a explains how the three-parameter kinematic model for a single shear span can be applied to an entire symmetrical two-span continuous deep girder subjected to two equal point loads. It is assumed that

the middle section of the beam does not rotate due to the symmetry of the structure. Starting from this section outwards the vertical displacement and rotation of the section at the load can be expressed from the kinematic model as follows:

(6) $\Delta = £_{t,avg}\, a \cot \sim + \Delta_c$

(7) $\ddot{} = \left(£_{t,avg} - £_{b,avg}\right)\cot \sim$

It can be seen that deflection Δ depends on the average strain along the top reinforcement between the loads while the rotation φ depends on the difference between the average strains in the top and bottom reinforcements in the internal shear span. The transverse displacement of the CLZ Δ_c increases the deflection but does not have an effect on the rotation. Knowing Δ and φ, the vertical displacement at the external support is expressed as:

(8) $\Delta_s = \Delta + \ddot{} \times a_{ext} - £_{b,avg}\, a_{ext} \cot \sim_{ext}$

Where the last term in the equation accounts for the deformations in the external shear spans subjected to single curvature. Because the external and internal shear spans experience the same maximum positive bending moment, the average strain along the bottom reinforcement $\varepsilon_{b,avg}$ is assumed to be the same in the two shear spans. It is further assumed that the transverse displacement of the external CLZs $\Delta_{c,ext}$ is negligible because the shear failure develops in the internal shear spans where the shear force is largest. With these simplifying assumptions the deformations of the entire continuous deep beam can be described with the help of only three independent parameters, namely $\varepsilon_{t,avg}$, $\varepsilon_{b,avg}$, and Δ_c. Furthermore, if the relative settlement of the supports Δ_s is zero, Equation (8) reduces the degrees of freedom to only two. In order to calculate the displacement field of the beam, equations (2)-(5) need to be evaluated in coordinate systems x'-z' and x"-z" attached to the sections at the loads. Coordinate system x'-z' is used for the external shear spans while x"-z" is used for the critical internal shear spans. The rotation and vertical translation of the two coordinate systems are given by Equations (6) and (7) while the horizontal translation away from the middle support is equal to $\varepsilon_{b,avg} \times h \times \cot \alpha$.

To demonstrate the accuracy of the kinematic model, equations (2)-(7) were applied to a 1200 mm deep continuous beam tested at the University of Toronto (Mihaylov et al. 2013b). The crack diagram of the beam with measured crack widths at shear failure is shown in Figure 2b. Below the crack diagram is the experimentally-obtained deformed shape depicted with a mesh of triangles (Figure 2c). The deformed shape was measured with the help of demountable displacement transducers (Zurich gauges) on a 300 mm by 300 mm grid of targets attached to the concrete surface. The values of the degrees of freedom of the kinematic model $\varepsilon_{b,avg}$, $\varepsilon_{t,avg}$, and Δ_c shown on the deformed shape were measured with linearly variable differential transformers (LVDTs). With these measured values the kinematic model produces the predictions shown with circles in Figure 2c. It can be seen that the circles match very well the measured locations of the Zurich targets corresponding to the vertices of the triangles of the deformed shape.

2. KINEMATIC THEORY FOR DEEP BEAMS

The kinematic model described above forms the basis of a three-parameter kinematic theory (3PKT) for predicting the ultimate shear behaviour of continuous deep beams (Mihaylov et al., 2013b). The kinematic model provides conditions for compatibility of deformations while the 3PKT also includes equations for equilibrium and constitutive relationships for the mechanisms of shear resistance in deep beams. The degrees of freedom of the kinematic model are calculated from:

(9) $£_{b,avg} \approx £_{b,\max} = \dfrac{M_r}{0.9 d_r \times E_s A_{sb}}$

(10) $£_{t,avg} \approx £_{t,\max} = \dfrac{M_l}{0.9 d_l \times E_s A_{st}} \geq 0$

(11) $\Delta_c = 0.0105 k_c l_{b1e} \cot\sim$

$k_c = 1/(0.8+170£_1) \le 1$

$£_1 = (1+\cot^2\sim)£_{t,\min} \ge 0$

Where bending moments M_r and M_l at the end sections of the shear span are usually expressed as a function of the unknown shear strength V. In the derivation of Equations (9) and (10) it is assumed that the longitudinal reinforcement remains elastic and that the lever arm of the internal longitudinal forces at the end sections is approximately 0.9 times the effective depth of the member. Equation (11), on the other hand, is derived based on assumptions for the size and shape of the critical loading zone, as well as assumptions about the distribution of the strains in the zone at shear failure (Mihaylov et al., 2013a). The size of the CLZ is characterized by the effective width of the loading element l_{b1e} = (V/P) $l_{b1.}$ Factor k_c accounts for the compression softening of the concrete in the CLZ caused by the tensile strain $\varepsilon_{t,min}$ in the top reinforcement near the load (Vecchio and Collins, 1986). Strain $\varepsilon_{t,min}$ can be taken equal to the average strain in the top reinforcement $\varepsilon_{t,avg}$ for members without stirrups and $0.75\varepsilon_{t,avg}$ for members with transverse reinforcement (Figure 1).

According to the 3PKT, the shear strength of deep beams can be expressed as a sum of four components:

(12) $V = V_{CLZ} + V_{ci} + V_s + V_d$

Where component V_{CLZ} is the shear carried by the critical loading zone, V_{ci} is the shear carried by aggregate interlock along the rough critical diagonal crack, V_s is the shear resisted by the stirrups, and V_d is the dowel action of the longitudinal reinforcement at the bottom of the critical diagonal crack. These mechanisms are expressed as functions of the deformations provided by the kinematic model, and thus as functions of the DOFs $\varepsilon_{t,avg}$, $\varepsilon_{b,avg}$, and Δ_c. The shear resistance of the critical loading zone V_{CLZ}, for example, similarly to the ultimate transverse displacement of the zone Δ_c, is proportional to the effective width of the loading element l_{b1e} and the compression softening factor k_c ($\varepsilon_{t,min}$). The aggregate interlock component, on the other hand, depends on the width of the critical diagonal crack *w* (Vecchio and Collins, 1986) which in turn depends on $\varepsilon_{b,min}$ and Δ_c. Similarly to $\varepsilon_{t,min}$, strain $\varepsilon_{b,min}$ can be taken equal to $\varepsilon_{b,avg}$ for members without stirrups and $0.75\varepsilon_{b,avg}$ for members with transverse reinforcement. The wider the diagonal crack, the less the interlocking of its rough surfaces. Term V_s is a function of the average strain in the stirrups $\varepsilon_{v,}$ which is also derived from the kinematic model. Finally, V_d depends on the tensile strain $\varepsilon_{b,min}$ within the length of the dowels l_k. The larger the tensile strain $\varepsilon_{b,min}$, the smaller the transverse capacity of the dowels. The derivation of the complete expressions for the four mechanisms of shear resistance in Equation (12) can be found elsewhere (Mihaylov et al., 2013a and 2013b). Shear strength calculations are performed individually for the two major diagonal cracks depicted in Figure 1. When calculations are performed for the top crack, the CLZ is at the support while the dowel action develops near the load at the top of the section. The minimum of the two shear resistances determines the final shear strength prediction of the 3PKT.

4. COMPARISONS WITH TESTS BY ASIN, 1999

The appropriateness of the three-parameter kinematic theory was examined with the help of fourteen tests of deep continuous beams reported by Asin 1999 (see also Asin and Walraven, 1995). The specimens had two spans of 2300 mm and were loaded by two equal point loads similarly to the beam discussed in Figure 2. The loads were applied at a distance of 1200 mm from the center of the middle support. The main variables were the depth of the section *h*, the distribution of the longitudinal reinforcement within the section, and the ratio of transverse reinforcement ρ_v, see Table 1. The depth of the section was either 1000 mm (beam names 1.0/) or 600 mm (beams 1.5/) with each of the two section types having a total amount of longitudinal reinforcement $A_{s,tot}=A_{s,bot}+A_{s,top}$ of 1080 mm^2 and 1352 mm^2, respectively. These amounts were distributed into top and bottom reinforcement according to the bending moments from a

linear elastic analysis (beams 1.0/1/ and 1.5/1/) or reversed (beams 1.0/2/ and beams 1.5/2/). Finally, each section type with a given depth and longitudinal reinforcement was provided with transverse reinforcement ratios varying between 0.20% and 0.50%. Ratio ρ_v of 0.20% corresponds to the minimum amount of web reinforcement required by the Canadian code (CSA Committee A23.3, 2004).

Table 1. Summary of tests.

Beam	a/d_{bot}	d_{bot}	d_{top}	h	$A_{s,bot}$	$A_{s,top}$	$f_{y,bot}$	$f_{y,top}$	f_c'	ρ_v	f_{yv}	V_{int}/P	V_{int}
	-	(mm)	(mm)	(mm)	(mm^2)	(mm^2)	(MPa)	(MPa)	(MPa)	(%)	(MPa)	-	(kN)
1.0/1/1	1.26	950	975	1000	452	628	586	567	26.8	0.50	569	0.663	518.0
1.0/1/1(r)	1.26	950	975	1000	452	628	586	567	29.6	0.50	569	0.658	529.0
1.0/1/2	1.26	950	975	1000	452	628	586	567	27.5	0.38	569	0.655	495.0
1.0/1/3	1.26	950	975	1000	452	628	586	567	25.8	0.22	569	0.652	388.0
1.0/2/1	1.23	975	950	1000	628	452	567	586	25.2	0.50	569	0.640	588.0
1.0/2/2	1.23	975	950	1000	628	452	567	586	28.2	0.38	569	0.630	469.0
1.0/2/3	1.23	975	950	1000	628	452	567	586	30.4	0.22	569	0.616	422.0
1.5/1/1	2.09	575	550	600	628	785	567	567	29.6	0.50	569	0.669	402.0
1.5/1/1*	2.09	575	550	600	628	785	567	567	29.9	0.48	581	0.662	348.0
1.5/1/2	2.09	575	550	600	628	785	567	567	28.9	0.38	569	0.665	347.0
1.5/1/3	2.09	575	550	600	628	785	567	567	25.9	0.22	569	0.657	261.0
1.5/2/1	2.18	550	575	600	785	628	567	567	27.8	0.50	569	0.642	375.0
1.5/2/2	2.18	550	575	600	785	628	567	567	26.0	0.38	569	0.631	339.0
1.5/2/3	2.18	550	575	600	785	628	567	567	28.5	0.22	569	0.642	246.0

For all specimens: Internal shear spans a=1200 mm; External shear spans a_{ext}=1100 mm; Section width b=150 mm; Width of external supports along the length of the beam = 200 mm; Width of middle support = 400 mm; Width of loading elements = 300 mm; Maximum size of course aggregate in the concrete a_g = 16 mm.

In order to apply the 3PKT approach to the critical internal shear spans of the specimens, it is necessary to know the distribution of the forces in the beam expressed by the ratio between the shear force in the internal shear span V_{int} and the load P. As the beam is statically indeterminate, the V_{int}/P ratio cannot be obtained from equilibrium equations alone. This ratio will be determined by applying the 3PKT in combination with Equation (8) for the differential settlement between the beam supports. For a chosen V_{int}/P value the 3PKT is used to calculate the shear strength of the internal shear span as well as deformations $\varepsilon_{b,avg}$, $\varepsilon_{t,avg}$, and Δ_c. These deformations are then used to calculate Δ_s from Equation (8). If the differential settlement is not equal to zero, the value of V_{int}/P is adjusted until the support conditions are satisfied. The value of V_{int}/P at which Δ_s equals zero corresponds to the predicted distribution of the forces in the continuous deep beam at shear failure.

The results from this procedure are shown in Figure 3 together with the V_{int}/P ratios measured in the fourteen tests. The experimental results show that the distribution of the forces in the specimens at shear failure depends mainly on the ratio $A_{s,top}/(A_{s,bot}+A_{s,top})$ which is plotted on the horizontal axis of the plot. The 3PKT predictions were obtained for averaged beam properties. According to the tests results the portion of the load transferred to the middle support increases slightly when the longitudinal reinforcement is redistributed from the bottom to the top of the section. This trend is captured by the 3PKT, even though the effect of the $A_{s,top}/(A_{s,bot}+A_{s,top})$ is slightly overestimated. The horizontal dotted line at V_{int}/P of 0.663 corresponds to a linear elastic solution based on the classical beam theory. It can be seen that this value agrees well with the experimental results and the 3PKT predictions for the specimens that were designed according to the linear beam model. Note also that the 3PKT line points towards a V_{int}/P value of about 0.5 as $A_{s,top}/(A_{s,bot}+A_{s,top})$ approaches zero. This result is consistent with the fact that a member with no top reinforcement will behave similarly to two separate simply supported beams after a flexural crack develops at the middle section.

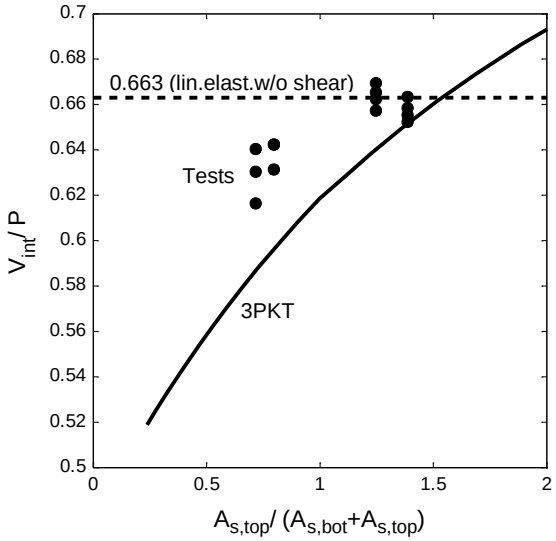

Figure 3. Distribution of support reactions at shear failure

Figure 4a compares the measured and predicted effect of the amount of stirrups on the failure load of the beams from the experimental study. The four groups of experimental points correspond to specimens with different section depths and distributions of the longitudinal reinforcement in the section. The test results show that the load-bearing capacity increased almost linearly as the ρ_v f_{yv}/ f_c' ratio was increased from about 0.04 to about 0.11. It can also be seen that the distribution of the longitudinal reinforcement in the section had a minor effect on the maximum load, while the 1000 mm deep specimens were significantly stronger than the 600 mm deep beams. These trends are captured very well by the 3PKT which is extrapolated up to ρ_v f_{yv}/ f_c' of 0.16. The linear increase of the failure load is predicted to continue up to ρ_v f_{yv}/ f_c'=0.15 which in the 3PKT is imposed as an upper limit on the amount of transverse reinforcement. It is assumed that larger amounts of stirrups will supress the shear failure along a diagonal crack and the member will fail due to crushing of the concrete in the web.

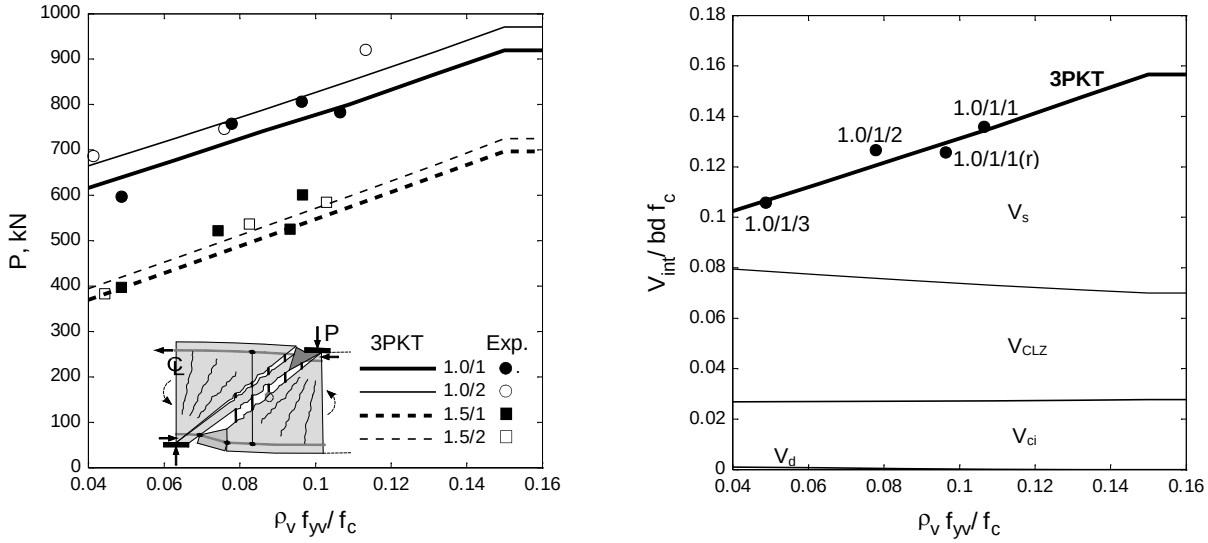

a) Load-bearing capacity b) Components of shear resistance

Figure 4. Strength predictions by the 3PKT

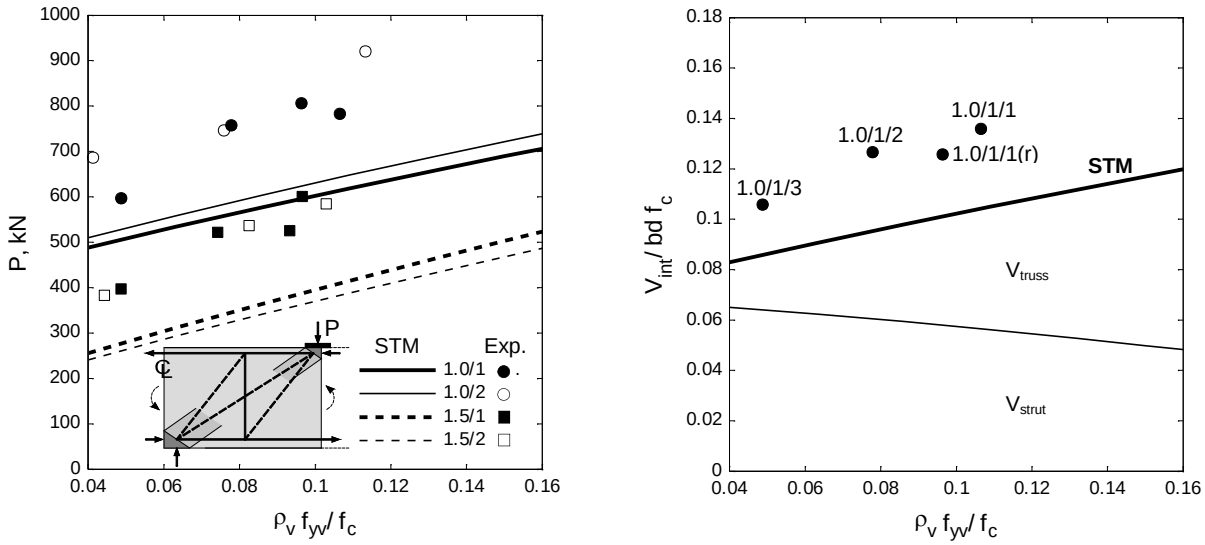

a) Load-bearing capacity b) Components of shear resistance

Figure 5. Strength predictions according to the CSA strut-and-tie model (STM) provisions

It is of interest to compare the 3PKT strength predictions to the predictions of the CSA strut-and-tie provisions, see Figure 5. The strut-and-tie model (STM) for the internal shear spans of the specimens is shown in Figure 5a with the dashed lines depicting the struts and the continuous lines depicting the ties. This model includes two-mechanisms of shear resistance: a direct diagonal strut that runs from the load to the support (strut action) and a mechanism with two parallel inclined struts and a vertical tie (truss action). The vertical tie, which represents the transverse reinforcement located within the middle one-half of the clear shear span, is assumed to yield prior to failure. The shear span is predicted to fail when the struts at the support or at the load crush. From Figure 5a it can be seen that the STM captures correctly the increase of the load-bearing capacity per unit increase of the $\rho_v f_{yv}/ f_c$' ratio but significantly underestimates the magnitude of the failure load. Figure 5b shows the predicted components of shear resistance V_{truss} and V_{strut} in the specimens with h=1000 mm and $A_{s,top}/(A_{s,bot}+A_{s,top})$=1.39. In comparing the STM and the 3PKT approaches, it can be assumed that V_{truss} in Figure 5b corresponds to V_s in Figure 4b, and V_{strut} in Figure 5b corresponds to $V_{CLZ}+V_{ci}$ in Figure 4b. It can therefore be concluded that the main difference between the two models is that STM accounts for the crushing in the CLZ and the aggregate interlock in a simpler and less accurate manner. The predictions of the two models and the experimental results are summarized in Table 2. Note that the STM calculations were performed with a V_{int}/P ratio of 0.663 as obtained from the linear elastic beam model without shear deformations. As shown at the bottom of the table, the 3PKT approach results in experimental-to-predicted shear strength ratios with an average value of 1.067 and a coefficient of variation (COV) of only 7.20%. The STM, on the other hand, produces an average value of 1.386 and a COV of 10.3%.

Finally, Figure 6 shows the complete measured load-deflection responses of specimens 1.0/2/1 and 1.5/2/1. The two solid dots in the plot show the 3PKT predictions of the ultimate load and ultimate deflection (displacement capacity) at shear failure of the internal shear spans. It can be seen that these predictions agree well with the measured ultimate response of the specimens. The 3PKT predictions are connected with straight lines to the points corresponding to first flexural cracking at the midspan sections. The cracking moment of the section is estimated based on the gross cross-sectional properties and a modulus of rupture $0.62\sqrt{f_c}$'. The load corresponding to the cracking moment and the deflection at cracking are obtained from a linear elastic beam model. It can be seen that a straight line approximation between the first cracking and the failure load significantly underestimates the stiffness of the member. The measured stiffness is higher mainly because of the gradual development of flexural and shear cracks, as well as due to the tension stiffening effect of the concrete between the cracks. Both these effects are negligible at failure where the 3PKT provides accurate predictions.

Table 2. Summary of test results and predictions

Beam	a/d_{bot}	f_c'	$\rho_v f_{yv}$	$A_{s,top}$	Experiment		CSA strut-and-tie (STM)			3PKT		
			f_c'	$A_{s,tot}$	V_{int}/P	V_{int}	V_{int}/P	V_{int}	V_{exp}	V_{int}/P	V_{int}	V_{exp}
	-	(MPa)			-	(kN)	-	(kN)	V_{pred}	-	(kN)	V_{pred}
1.0/1/1	1.26	26.8	0.11	1.39	0.663	518.0	0.663	397.9	1.302	0.659	515.0	1.006
1.0/1/1(r)	1.26	29.6	0. 10	1.39	0.658	529.0	0.663	420.6	1.258	0.660	532.3	0.994
1.0/1/2	1.26	27.5	0.08	1.39	0.655	495.0	0.663	372.1	1.330	0.653	470.4	1.052
1.0/1/3	1.26	25.8	0.05	1.39	0.652	388.0	0.663	317.6	1.222	0.647	399.3	0.972
1.0/2/1	1.23	25.2	0.11	0.72	0.640	588.0	0.663	397.3	1.480	0.584	469.2	1.253
1.0/2/2	1.23	28.2	0.08	0.72	0.630	469.0	0.663	390.5	1.201	0.582	445.5	1.053
1.0/2/3	1.23	30.4	0.04	0.72	0.616	422.0	0.663	365.1	1.156	0.580	407.8	1.035
1.5/1/1	2.09	29.6	0.10	1.25	0.669	402.0	0.663	265.9	1.512	0.642	353.0	1.139
1.5/1/1*	2.09	29.9	0.09	1.25	0.662	348.0	0.663	263.3	1.322	0.642	348.8	0.998
1.5/1/2	2.09	28.9	0.07	1.25	0.665	347.0	0.663	226.1	1.534	0.638	302.1	1.149
1.5/1/3	2.09	25.9	0.05	1.25	0.657	261.0	0.663	168.0	1.553	0.629	233.6	1.117
1.5/2/1	2.18	27.8	0.10	0.80	0.642	375.0	0.663	251.6	1.491	0.605	355.9	1.054
1.5/2/2	2.18	26.0	0.08	0.80	0.631	339.0	0.663	210.2	1.613	0.601	302.0	1.122
1.5/2/3	2.18	28.5	0.04	0.80	0.642	246.0	0.663	171.3	1.436	0.595	248.3	0.991
								Avg.=	1.386			1.067
								COV=	10.3%			7.20%

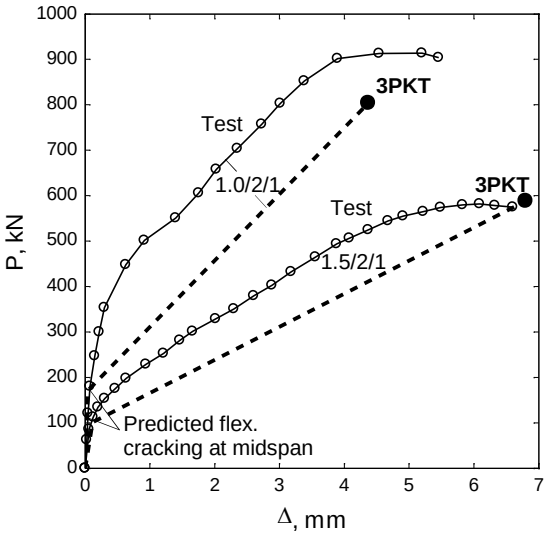

Figure 6. Load-displacement response

4. SUMMARY AND CONCLUSIONS

This paper presented a simple macro-kinematic description of the deformation patterns in diagonally-cracked continuous deep beams. It was shown that symmetrical two-span members subjected to two equal point loads can be modelled accurately with the help of only three degrees of freedom. These degrees of freedom are the average strain in the top reinforcement between the loads, the average strain in the bottom reinforcement along the entire member, and the transverse displacement of the critical loading zones. By considering a zero relative settlement of the beam supports, the degrees of freedom were further reduced to two. The kinematic model forms the bases of a three-parameter kinematic theory (3PKT) which was used to study the ultimate behaviour of fourteen shear critical test specimens from the literature. The test variables were the depth of the member, the ratio of top to bottom longitudinal reinforcement, and the amounts of transverse reinforcement. It was shown that the effects of these

variables were well predicted by the 3PKT approach. The experimental-to-predicted shear strength ratios had an average value of 1.067 and a coefficient of variation (COV) of only 7.20% compared to an average value of 1.386 and a COV of 10.3% produced by the CSA strut-and-tie model. It was also shown that the 3PKT approach can be used to predict the support reactions and the displacement capacity of shear critical continuous deep beams. Further research is needed to extend the approach to model the complete load-displacement response of such members.

References

ACI Committee 318 (2008) Building Code Requirements for Reinforced Concrete (ACI 318-08) and Commentary (318R-08), American Concrete Institute, Farmington Hills, Mich., 465 pp.

Asin, M. (1999) The Behaviour of Reinforced Concrete Continuous Deep Beams, Doctoral Thesis, Delft University Press, The Netherlands.

Asin, M. and Walraven, J. (1995) Numerical Analysis of Reinforced Concrete Continuous Beams, *HERON*, 40: 163-178.

CSA Committee A23.3 (2004) Design of Concrete Structures, Canadian Standards Association, Mississauga, Ontario, Canada, 214 pp.

European Committee for Standardization, CEN, EN 1992-1-1 (2004) Eurocode 2: Design of Concrete Structures- Part 1-1: General Rules and Rules for Buildings, Brussels, Belgium, 225 pp.

Mihaylov, B., Bentz E. and Collins, M.P. (2013a) Two-Parameter Kinematic Theory for Shear Behaviour of Deep Beams, *ACI Structural Journal*, 110: 447-456.

Mihaylov, B., Hunt, B., Bentz, E. and Collins, M.P. (2013b) Three-Parameter Kinematic Theory for Shear Behaviour of Continuous Deep Beams, *ACI Structural Journal*, submitted.

Vecchio, F.J. (2001) Disturbed Stress Field Model for Reinforced Concrete: Formulation, *ASCE Journal of Structural Engineering*, 127: 12-20.

Vecchio, F.J. and Collins, M.P. (1986) The Modified Compression Field Theory for Reinforced Concrete Elements Subjected to Shear, *ACI Journal*, Proceedings, 83: 219-231.